Mechanisms for Identification of Micro-objects Based on the Use of Characteristics in the Image Structure

Rustam A. Safarov[1,2(✉)], Isroil I. Jumanov[3], Olimjon I. Djumanov[3], and Umid Z. Djumayozov[2]

[1] Tashkent University of Information Technologies named after Muhammad al-Khwarizmi, Tashkent, Uzbekistan
rustammix.rs@gmail.com

[2] Samarkand branch of Tashkent University of Information Technologies named after Muhammad al-Khwarizmi, Samarkand, Uzbekistan

[3] Samarkand State University named after Sharof Rashidov, Samarkand, Uzbekistan

Abstract. Scientific and methodological foundations, methods, and mechanisms for optimizing the processes of identification, recognition, and classification of micro-objects (pollen grains and single-celled organisms) have been developed using tools that utilize dynamic, statistical, geometric, morphological, and signal characteristics of images. The study examines control systems for industrial and technological complexes, palynology, environmental and ecology monitoring, and medical diagnostics. Methods for optimizing micro-object image identification are proposed, based on tools for adjusting parameter values for image point changes, adjusting network structure, variable activation functions, and filtering models for noise, random outliers, and image spikes. Estimates of the root-mean-square error were obtained for various dynamic image identification models combined with a three-layer neural network. A software package for optimizing the processes of identification, recognition, and classification of micro-objects was implemented and tested using data obtained during the diagnosis of tuberculosis patients. Three-layer, recurrent, loosely coupled neural network modules, along with supervised and unsupervised network learning algorithms, were used. The effectiveness of the proposed approaches is substantiated by improved recognition accuracy and resilience to noise-induced image distortions. A comparative analysis of existing micro-object processing methods is conducted, identifying their limitations and the advantages of the developed solutions. It has been demonstrated that integrating various image characteristics and adaptive learning models can improve classification accuracy in complex environments. The results can be used in biomedical research, environmental monitoring, and automated diagnostic systems.

Keywords: Image · Micro-object · Identification · Recognition · Classification · Optimization · Error · Software Package · Probability

© The Author(s), under exclusive license to Springer Nature Switzerland AG 2027
O. Gervasi et al. (Eds.): ICCSA 2026 Workshops, LNCS 16758, pp. 117–132, 2027.
https://doi.org/10.1007/978-3-032-30497-1_8

1 Introduction

In the control systems of production and technological complexes, monitoring of the environment and ecology of the region, palynology, medicine and other fields of knowledge, micro-objects of various types are used, for example, pollen grains, unicellular microorganisms, minerals in rock mass, food products and others [1–3]. Existing technologies for processing images of micro-objects are focused on the functions of counting, analysis, identification, recognition, and classification of micro-objects, which are not performed quickly enough, with high error rates and costs [4–7].

Improvements are needed in processing information from micro-objects presented for use in digital, video, photo, and luminance images, as well as in identifying the desired characteristics in the informative portion of a colour image. The development of effective tools for filtering and correcting defective points in micro-object images, and the use of combined dynamic models and neural networks (NN) for this purpose, are also required [8–11].

Of great scientific significance is the research and development of constructive approaches, principles, and methods for identification, recognition, and classification of micro-objects through the use of statistical, dynamic, morphometric, textural, colour, brightness, spectral and frequency characteristics of the image [12–14].

This work is devoted to the research and development of a methodology for optimizing the processes of identification, recognition and classification of micro-objects based on problem-oriented information processing systems.

2 Related Work

In recent years, methods of using modern computer vision systems (CVS) and intelligent technologies for analysing and processing information based on the mathematical apparatus of soft computing and dynamic models for identifying micro-objects have been widely developed [15–17].

Scientific achievements in this field are mainly based on approaches that use classical methods of processing images of micro-objects, as well as on methods of optimal problem-oriented information processing that apply deep machine learning algorithms and tools, such as YOLOv8 models [18–20]. Classical approaches represent a wide class of algorithms that perform such functions as contour selection, reference points, segmentation, extraction of informative features, statistical and dynamic properties of information, as well as the use of geometric, textural and brightness characteristics of image points [21–23].

Methods using neural networks and their hybrid architectures combined with dynamic models are becoming increasingly widespread. Hybrid models have been shown to automatically generate information points in a sequence, providing higher accuracy in recognizing and classifying micro-objects with lower processing costs. At the same time, their use is justified by the need to replace existing technologies, which rely on significant computing resources and large data volumes [24–26]. Combined approaches that combine traditional image processing

methods with NNs are aimed at increasing the stability of algorithms, eliminating noise and defective points, as well as distorted information [27,28].

Thus, despite significant progress in the subject area under study, existing methods, algorithms, and software applications do not fully ensure the required accuracy and reliability of information processing. This underscores the importance and relevance of the problem of identifying, recognizing, and classifying micro-objects based on problem-oriented information processing systems using the characteristics of image structural components.

3 Materials and Methods

3.1 Tools for Optimizing Micro-object Identification Based on Filtering and Detection of Defective Image Points

An approach aimed at identifying micro-objects is proposed, based on the use of component characteristics in the image structure and the development of tools for high-precision image point reconstruction using the following operators:

Shift transformation, parameter determination, and colour coding of image points;

Color visualization of micro-objects, representation of the use of geometric, textural, and morphometric image characteristics;

Creation of edge maps, segment centres, and image cores.

Various noise reduction filters were researched and implemented, used to highlight specific areas of an image or remove other components. This involved determining the nature of the noise, the image's dynamic range, the colour accuracy, and identifying many other factors that negatively impact filtering results.

Gaussian and median filters were studied, demonstrating the best performance in suppressing noise and impulse interference, preserving the sharpness of the boundaries of contrasting parts of the image of micro-objects, and replacing the spectral intensity with pixels of a point located near the median [29–31]. The filtering tool, correction of defective points, and conditions caused by shifts, blurring, and distortions of information are taken into account when solving the equation

$$I_{\text{new}}(x, y) = \underset{(kx,ky)\in K_{xy}}{\text{med}} \{I_{\text{old}}(kx, ky)\}$$

where I_{new} and I_{old} - new and old pixel values of the image point;

K_{xy} – image point sizes in pixels; $K_{Hs} \times K_{Ws}$ – kernel center with window, tracked point (x, y). It is important to filter out additive noise in the contour of image points. For this purpose, a Gaussian filter was implemented, based on a combined three-layer neural network model and a discrete wavelet transform

$$I_{\text{new}}(x, y) = \sum_{dx=-RH}^{RH} \sum_{dy=-RW}^{RW} G(dx, dy) \cdot I_{\text{old}}(x + dx, y + dy),$$

where G – filter function of the combined Gaussian model; RH and RW – constants of the filter rank, respectively, vertically and horizontally;

$$I_{\text{new}}(x,y) = \frac{1}{\sqrt{2\pi}\,\sigma} e^{-\frac{x^2}{2\sigma^2}} \times \frac{1}{2\pi\,\sigma^2} e^{-\frac{y^2}{2\sigma^2}},$$

- combined Gaussian distribution of additive noise and useful point; x, y - distances from the origin of coordinates along the abscissa and ordinate axes, in which the values of the signal/noise parameter are measured;

σ – error (mean-square deviation) of filtering the image of micro-objects.

The additive image noise filtering tool under study also combines operators for detecting and correcting defective points. Four regions are considered: LL, HL, LH and HH. The results of the YOLOv8 application are generated and represented as data matrices.

The results of the correction of defective points are presented in the area LL, the values of which are determined by the row and column of the data matrix. The complexity of the image texture, which is caused by interfering factors, in turn, hinders the high-precision identification of micro-objects. Solving the problem is further complicated when the models describing the influencing factors have a nonlinear structure.

To solve the network training problem, the initial point of the image signal is defined, taking into account the impact of noise and factors leading to defective points. The signal model of an image point is generally defined as

$$Z(n) = X(n) + E(n),$$

where $X(n)$ is a useful signal of the image point; $E(n)$ is an error, the value of which is determined by the influence of the signal/noise parameter and defects due to blurring, shifts in points of information distortion and other reasons. The neural network training algorithm is optimized using a tool based on the vector definition operator $W = [w_0, w_1, \ldots, w_k]^T$, where T is the set of neuron weight values in the network's input layer.

The filtering tool for applying nonlinear wavelet analysis schemes is based on the model [32,33]

$$X_M(n) = \sum_{(j,k)\in I_M} \langle X, Y_{j,k}(n)\rangle\,,$$

where $\Psi_{j,k}(n) = 2^{j/2}\,\Psi\left(2^j n - k\right)$ – component of the orthogonal basis; I_M – a set of indices of dimension M. If expression represents wavelet coefficients in the space of the wavelet function, then it is given in the form

$$W_{j,k}(Z) = X_{\Psi_{j,k}} + E_{\Psi_{j,k}},$$

where $X_{\Psi_{j,k}} = \langle X, \Psi_{j,k}\rangle\,, \quad E_{\Psi_{j,k}} = \langle E, \Psi_{j,k}\rangle$.

Which are implemented based on the threshold function

$$X_M(n) = \sum_{j,k} P_T(\langle Z, \Psi_{j,k}\rangle)\,\Psi_{j,k}(n),$$

and the indicator

$$P_T(x) = \begin{cases} x, & \text{if } |x| \geq T; \\ 0, & \text{if } |x| < T, \end{cases}$$

where T - threshold; σ^2 – noise variance, the value of which is estimated by the median

$$\sigma^2 \approx \text{Med}(\langle Z, \Psi_{j,k} \rangle)_{0<k<\frac{N}{2}} .$$

Figure 1 a), b) shows graphs of the dependencies of the probability of detecting defective points P_d for two curves: a) signal 1, b) signal 2. The solid curve corresponds to the result of the traditional algorithm, and the dashed-dotted curve corresponds to the result of the developed tool.

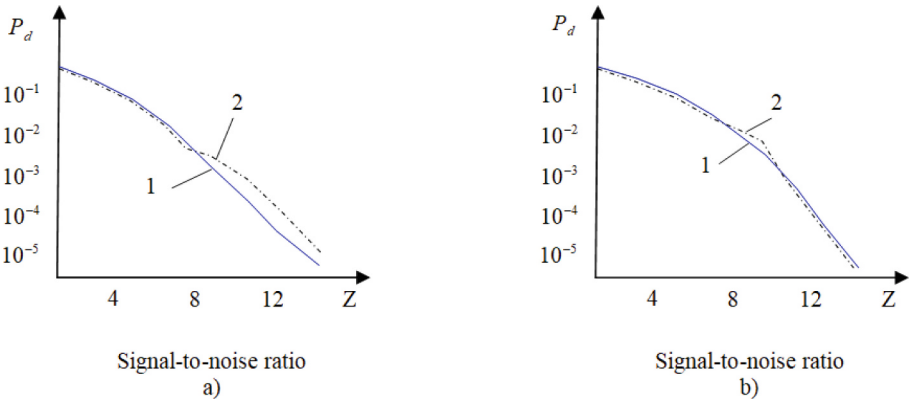

Fig. 1. Efficiency of defective point detection a) signal 1 b) signal 2.

It is determined that the probability of detecting defective image points varies depending on the training steps. In experimental studies, a hybrid model with a generalized algorithm was tested with an iteration step of 0.01. The graph of the traditional algorithm, plotted based on the values of the signal-to-noise Z parameter, almost converges with the curve of the proposed optimization tool for correcting distorted information from micro-objects.

The error function $H(U)$ at the threshold point of the neuron activation function exhibits a discontinuity of the first kind. The neuron weighting coefficients do not ensure an exact repetition of the signal shape. The main feature of the tool is the optimization of training sets, taking into account variations in their size.

To achieve high-precision image identification, the YOLOv8 tool was used. In this tool, the number of neurons in the layers and the network layers are adapted during deep learning, and a fixed threshold on the activation function is tuned from initial values.

A tool for optimizing image identification processes was developed based on YOLOv8 deep learning algorithms, which are tuned by adapting the size and properties of texture characteristics in the generated training set.

Figure 2 demonstrates the study's results, demonstrating the 99.6% recognition and classification accuracy achieved using the YOLOv8 model, as demonstrated on a validation set containing four pollen grain classes. The horizontal axis (True) indicates the true object classes, and the vertical axis (Predicted) indicates the classes predicted by the model.

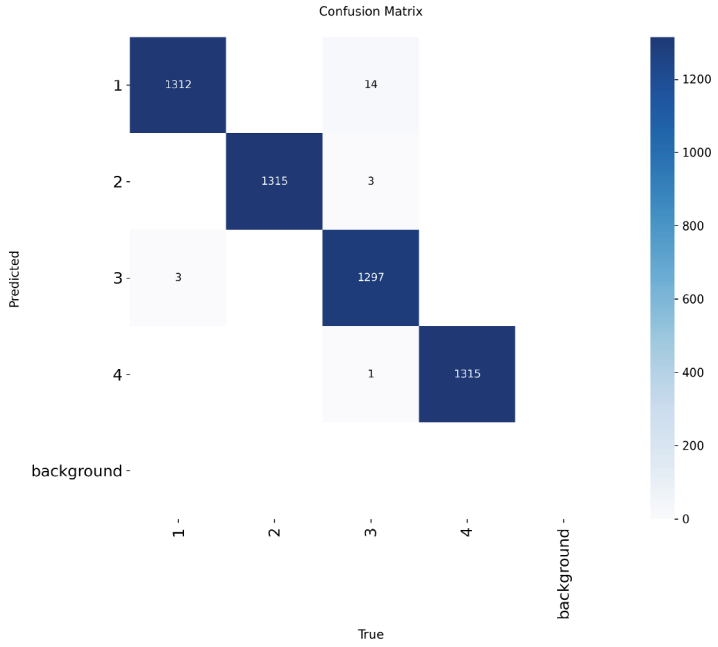

Fig. 2. Classification of micro-objects based on YOLOv8 and the error matrix.

Values on the main diagonal correspond to correctly classified samples: Class 1 – 1312 samples, Class 2 – 1315, Class 3 – 1297, and Class 4 – 1315. Values off the diagonal indicate misclassifications: the highest number of errors is observed for Class 1, where 14 samples were incorrectly classified as Class 3. Class 2 has three samples incorrectly classified as Class 3, Class 3 has three samples incorrectly classified as Class 1, and one sample is incorrectly classified as Class 4. Class 4 exhibits the lowest number of interclass errors – only one sample was incorrectly classified as Class 3. The "background" row and column are left blank, indicating the absence of false positives for background objects. The total number of correctly classified samples was 5239 out of 5260, corresponding to an overall model accuracy of 99.6%.

In another version of the study, the adaptive deep learning algorithm of the neural network is combined with modules of the wavelet package, which

allows removing the noise part from the image structure and identifying the used characteristics of the components.

Figure 3 shows the performance graphs of the identification tool with filtering, correction of defective points, and distorted information, as measured by the function T versus the complexity of information processing. The curve dynamics depend on the number of filter stages N.

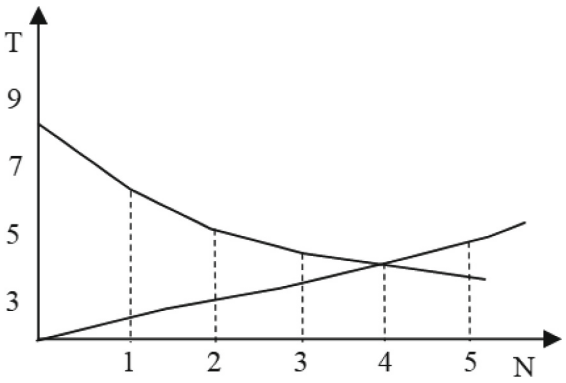

Fig. 3. The complexity of processing information of the tool.

Curve 1 corresponds to the filter with the image point tracking kernel adaptation tool, and curve 2 corresponds to the two-dimensional discrete Fourier transform without using the identification optimization tool. Curve 2 of the T function increases linearly with the increase in the number of stages of the pyramidal model in the multi-stage adaptive filter (MAF). Curve 1 corresponds to the application of the MAF model without the image point kernel adaptation tool. With parameter values of $N = 4$ and $T = 1.2 \cdot 10^6 \text{op}/\mu\text{s}$, the computational cost of problem-oriented information processing decreases approximately 15-fold.

3.2 Tools For Optimizing Micro-object Identification Based on Filtering and Correction of Defective Image Points

Tools have been developed to optimize micro-object identification processes, expanding the capabilities of the previous image processing tool based on filtering operators, defect point correction, selection, and adaptive segmentation of image contours.

The image contour tool divides the image into a number of regions with similar point characteristics. The contour is then segmented based on the matching of similar point characteristics, such as intensity, brightness, colour, and texture. A CNN is used for adaptive image contour segmentation [34,35].

Noise filtering and defect point correction tools are synthesized with parallel information processing algorithms that include self-tuning tools. To optimize the

identification of micro-objects with filtering and correction of defective points, a one-dimensional mapping of the input image with a point x and its activation neural function was used [36,37]

$$f(x) = \frac{\mu}{1 + exp(-\alpha x + \beta)},$$

where α - slope coefficient, $\alpha > 0$; β - displacement values, μ - magnification factor, $\mu > 0$.

For optimization, the values of parameters α and β are chosen so that the range of input image points $[x_{\min}, x_{\max}]$ is mapped to one neuron and is located between the values of the unstable point x_1^* and one of the two stable points x_2^*. The input values of the variable are grouped according to their degree of proximity, and this operation continues until a stable point with a minimum training error of the CNN E is reached.

Parameters α and β are determined from the system of equations

$$x_i^* = f(x_i^*, \alpha, \beta, \mu), \quad i = 1, 2.,$$

where x_i^* are the values of the input variable that are associated with the definitions of the verification limits in the range $[x_{\min}, x_{\max}]$ in the form of the following relationships:

$$x_1^* = x_{\min} - \delta_1, \quad x_2^* = x_{\max} - \delta_2, \quad |\delta_1| \ll 1 \text{ and } |\delta_2| \ll 1.$$

The system of equations is solved for α and β only if the value of the coefficient μ is increased or specified in advance.

The solution to this system of equations is obtained in the form:

$$\alpha = \frac{1}{x_2^* - x_1^*} \ln\left(\frac{(\mu - x_1^*)x_2^*}{(\mu - x_2^*)x_1^*}\right), \quad \beta = \alpha x_1^* + \ln\left(\frac{\mu - x_1^*}{x_1^*}\right).$$

The neural network training optimization tool, based on information about changes in parameter μ, adjusts the values of parameters α and β, and then selects activation functions for the network neurons. To optimally select stable points when identifying micro-object images, the value of parameter μ is set in the neighbourhood of $\max|\Delta H|$, which is estimated using Shannon's unconditional and conditional entropy formula ΔH.

In experimental studies, the entropy of H image pixel intensities was calculated for each value of parameter μ. The entropy sequence was determined to depend on the values of parameter μ. As a result, it was proposed that the values μ_0 corresponding to $\max|\Delta H|$ be used to determine cluster boundaries in image pixel intensities. This result demonstrates the greatest increase in average useful information obtained by changing the value of parameter μ.

Figure 4 shows a graphical comparison of the efficiency of the tool for optimizing the identification of micro-object images using the function $K = T_{opt}/T_{tr}$ - the gain coefficient in the complexity of information processing, where T_{opt} is the gain coefficient for the MAF and variable adaptation operators.

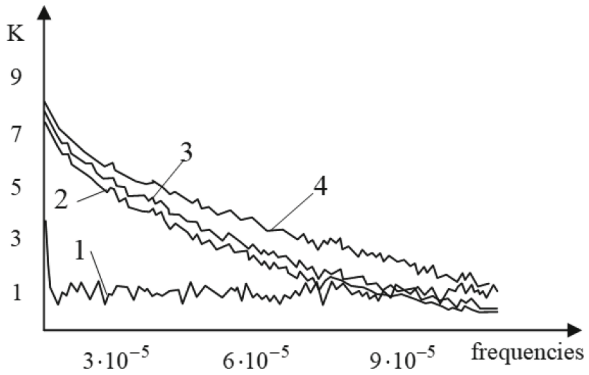

Fig. 4. Tuning efficiency in time and frequency domain.

The graphs were obtained for different signal frequency values L for three- and nine-channel filtering. Curve 1 corresponds to a traditional normalized linear MAF, curve 2 corresponds to a three-channel MAF, curve 3 corresponds to a nine-channel MAF, and curve 4 corresponds to a MAF-based instrument.

4 Results and Discussion

4.1 Results of Preliminary Processing of Images of Micro-objects

The most suitable format for colour video images is RGB, which utilizes three parameters of each pixel in the image frame. Rotating the image edge away from the light source changes the illumination of each point, requiring the R, G, and B variables to be fixed within a specific range of values [38].

Each point in the image contour of micro-objects is represented by the values of the solid line R, dashed line G, and dash-dotted line B parameters, which are determined by a high-resolution pixel matrix. Increasing the pixel intensity of a point increases the illumination of each image point, while decreasing the pixel intensity of a point reduces its illumination.

Table 1 shows the average values of quantitative characteristics of image points in a palette of $M = 16777216$ colours, measured over a period of 3 months.

The spectral range of signal characteristics of colour image points of micro-objects was studied using a method that helps determine the boundary, shape, and cross-sectional area of each point. Changes in point brightness along a line from one edge (cross-section) to the other are determined using statistical analysis or fuzzy logic [39].

Statistical analysis allows us to establish the main characteristics of the material flow at a specific point, time period, and time of analysis of colour images, which are used to determine the mineral composition of products on the conveyor.

Table 1. Brightness estimates for a colour image point of micro-objects

Time in days	R	G	B	NR	NG	NB	Number M
1–15	168	154	140	0.34595	0.00010	0.00000	341
15–30	165	162	152	0.13938	0.00000	0.00000	583
30–45	163	158	130	0.22650	0.00004	0.00000	184
45–60	159	139	119	0.53682	0.00011	0.00001	352
60–75	164	140	139	0.37499	0.00000	0.00000	431
75–90	140	143	125	0.23675	0.00001	0.00000	104
90–105	137	125	131	0.11207	0.00056	0.00000	231

The experimental studies examined medical objects using 450 digital microscopy images of 10 sputum smears. RGB and HSV color images were analyzed.

It was determined that the implemented mechanisms for identifying single-celled organisms significantly improve the speed and reliability of image parameter values for microscopic objects.

Sputum from patients with pulmonary tuberculosis was used to prepare the smears.

Sputum is stained red for acid-fast bacilli, and other elements in the sputum are stained blue.

In each image, pixel parameters were calculated with the following values: Red pixel color (R); Green pixel color (G);

Blue pixel color (B); Pixel brightness (Y);

Pixel hue (H); Pixel saturation (S); Pixel value (V).

Each pixel of the image point was represented by 7 parameters: R, G, B and Y in the range of values from 0 to 255; H in the range of 0 to 360; S and V in the range of 0 to 100.

All 450 images are divided into a training set of 314 images, a test set of 68 images, and a control set of 68 images.

Table 2 shows the spectral portion of the RGB image with background reflections of its parts: left (solid line), middle (dashed line), and right (dash-dotted line).

Figures 5 a), b) illustrate the probabilistic characteristics of the tools for optimizing the identification, recognition, and classification of micro-objects. A) the results are presented based on the point values of function $P_i = n_i/N_i$ — correct recognition and classification of micro-objects; b) the results are obtained depending on various values of parameter $\mu = \lambda\tau$ —function $hatP_i$ —the intensity of RGB image pixel intensity. The background of the image pixel is reflected. The left part is solid, the middle part is dashed, and the right part is dashed-dotted lines.

Figure 5 a) illustrates the probabilistic characteristics of the implemented mechanisms for identification, recognition and classification of micro-objects,

Table 2. Estimates of spectral characteristics of micro-object images

Time in days	R	G	B	Left side	Middle part	Right side	Number M
1–15	168	154	140	1.1062	17.7000	33579	341
15–30	165	162	152	1.1007	0.00000	32157	583
30–45	163	158	130	1.1067	0.00004	32204	184
45–60	159	139	119	1.1072	0.00011	32267	352
60–75	164	140	139	1.1115	0.00000	32204	431
75–90	140	143	125	1.1110	0.00001	32575	104

which are assessed according to the criterion of correct image recognition by one point

Figure 5 b) shows graphs of the function, which are plotted against parameter—the intensity of the RGB image pixels. The graph reflects the image background: the left part (solid line), the middle part (dashed line), and the right part (dashed-dotted line).

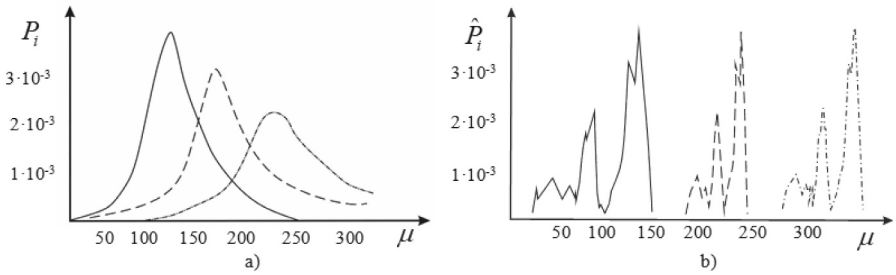

Fig. 5. Probabilities of image point recognition.

The values of R, G and B were determined using the relationship:

$$Y = 2.299 * R + 0.587 * G + 0.114 * B.$$

During testing of the mechanisms, the minimum and maximum boundaries of parameters H, S and V were determined, within which the pixels of the dots were related to acid-fast mycobacteria, while the values outside these boundaries are considered to relate to other objects. The following results were established: upper bound for parameter $H = 360$; upper bound for parameter $S = 70$; lower bound for parameter $V = 70$; upper bound for parameter $V = 100$.

Two neural networks were constructed to improve the accuracy of micro-object image identification. The first of these is used to select the best image characteristic based on 191 parameters of the lower bound of H, the second is of the lower bound of S. The most optimal neural network topology was

determined, which has 14 neurons in the input layer, 14 in the hidden layer, and 1 in the output layer.

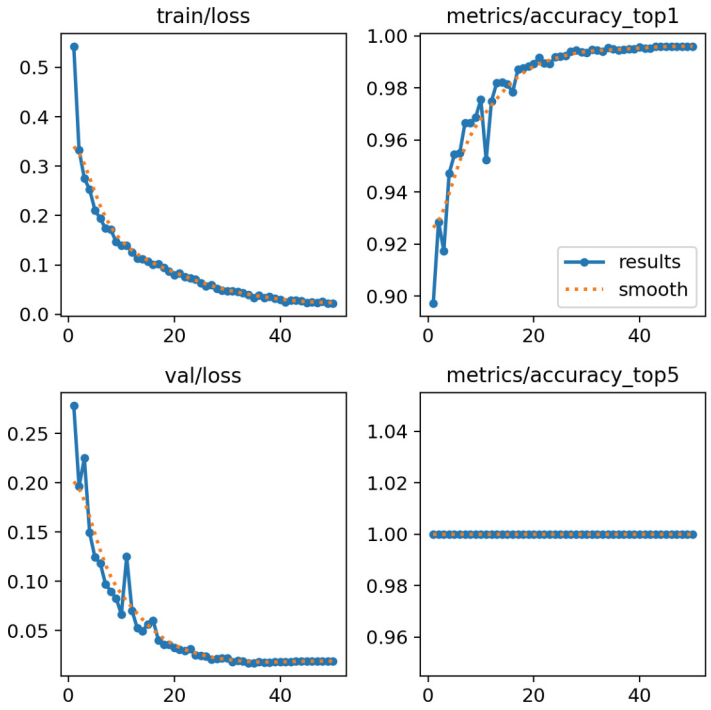

Fig. 6. YOLOv8n training graphs: loss functions and classification accuracy metrics over 50 epochs.

4.2 Implementation of Research Results

Figure 6 illustrates the YOLOv8 training graphs, which are evaluated by the value of the loss function for classifying a micro-object depending on different observation epoch lengths.

Graph 1—train/loss—shows the dynamics of the loss function on the training set. In the initial stage (epochs 1–5), a sharp decrease in loss is observed from 0.54 to 0.15, indicating intensive model training. Subsequently (epochs 5–50), the decrease becomes gradual and stable, reaching a value of approximately 0.02–0.03 by the end of training. The smoothed curve (orange dotted line) confirms the uniform and stable nature of the loss function's decrease, with no signs of divergence. This trend indicates correct model convergence during training.

Graph 2—metrics/accuracy/_top1—shows the change in Top-1 classification accuracy on the validation set across epochs. At the beginning of training (epochs 1–3), accuracy was approximately 0.90, after which minor fluctuations

were observed due to the initial adjustment of the model weights. Beginning with epoch 5, a steady increase in accuracy is observed: by epoch 20, it reaches a level of 0.98–0.99, and by epoch 50, it reaches a maximum value of 0.995. The smoothed curve demonstrates a general upward trend with gradual stabilization at 0.99 at the end of training. Fluctuations in results between epochs are due to the stochastic nature of the training process and the data augmentation methods applied.

Graph 3—val/loss—displays the dynamics of the loss function on the validation set. In the first epochs, a significant decrease in loss is observed, from 0.27 to 0.08, similar to the trend on the training set. Moderate fluctuations with local peaks of 0.12–0.21 are observed around epochs 10–15, after which, starting from epoch 20, the curve stabilizes in the range of 0.02–0.03. Importantly, the validation set does not demonstrate a sustained increase in the loss function compared to the training set, indicating the absence of significant overfitting of the model. The patience parameter of 20 ensured continued training during periods of temporary performance degradation.

Graph 4—metrics/accuracy_top5—shows the Top-5 classification accuracy on the validation set, which remains at 1.00 throughout the training process. This result indicates that in all cases, the true class was among the five most probable model predictions. The reliability of the result is explained by the fact that the classification task considers only four classes. Therefore, the achieved Top-5 accuracy of 1.00 is reasonable, confirming the correctness of the model's performance and the accuracy of the data labeling.

The hyperbolic tangent function is used as the activation function for the neurons in the hidden layer of the network, and an exponential function is used for the output layer. On a validation training sample, the neural network's mechanisms provide identification accuracy of up to 97.5%, with a maximum error rate of 2.5% for micro-objects.

Table 3 shows the results of testing dynamic models combined with CNN – Daubechies wavelet analysis, 4, and a generalized network training algorithm.

Table 3. Results of hybrid models for micro-object image identification

Sets	Identification error in%	Probability of recognition error in %	Average classification error in %
Educational	97.9	2.1	1.87
Test	98.5	1.5	1.51
Control	97.5	2.5	2.27

It was determined that when training neural network algorithms based on the lower bound of S, in which the network has 8 neurons in the input layer, 7 in the hidden layer, and 1 in the output layer, the hybrid neural network training algorithm on the training set performs with an error of 89.4%. Moreover, the highest probabilistic recognition error is 10.6%, and the average micro-object classifica-

tion error is 6.3%. The training performance of the hybrid neural network model on the test and validation sets is virtually identical.

Table 4 shows the results of the combined neural network training algorithm.

Table 4. Test results of the NN training algorithm for the hybrid model

Sets	Identification error in %	Probability of recognition error in %	Average classification error in %
Educational	89.4	10.6	0.63
Test	90.8	9.2	0.45
Control	90.1	9.9	0.57

A software package for the identification, recognition, and classification of micro-objects was developed and implemented. It utilizes morphometric, geometric, colour-brightness, and spectral image characteristics. The average processing time for a single image was found to be 9.532 µs, and for 450 images with a resolution of 572×422 pixels, it was nearly 42.75 µs. The average time spent filtering and correcting defective image points was 9.266 µs. The average neural network training time was 0.006 µs.

5 Conclusion

Scientific and methodological foundations, methods and algorithms for optimizing the identification, recognition and classification of micro-objects have been developed based on tools for using statistical, dynamic, morphometric, textural, color and brightness characteristics of the image of micro-objects.

The developed algorithms enable processing information about the three-dimensional structure of a micro-object, estimating its spatial position, and localizing desired objects in the image. Tools for optimizing micro-object identification are proposed, including the selection, filtering, and correction of defective image points, based on the extraction of local features and characteristics of heterogeneous fragments.

The mathematical apparatus for training neural networks was used at the stages of pre-processing, segmentation of microscopic digital images of sputum, recognition of objects (acid-fast mycobacteria), and diagnosis of tuberculosis. It was also implemented in clinical practice, the results of which demonstrate an obvious improvement in the quality of microbiological diagnosis of tuberculosis.

The YOLOv8 model demonstrated high performance in classifying microobjects: Top-1 accuracy was 99.5%, Top-5 accuracy was 100%, and the overall error matrix accuracy reached 99.6% (5239 out of 5260 samples) with no signs of overfitting, confirming the suitability of the model for automated analysis of microscopic images.

The theoretical results of the study are of practical interest in the design of problem-oriented information processing systems and the creation of a modified

computer vision technology for images of pollen grains, as well as images of minerals in rock mass.

References

1. Sonka, M., Hlavac, V., Boyle, R.: Image Processing, Analysis and Machine Vision. Springer, New York (2013). https://doi.org/10.1007/978-1-4899-3216-7
2. Marcos, J.V., et al.: Automated pollen identification using microscopic imaging and texture analysis. Micron **68**, 36–46 (2015)
3. Philipp, V., König, M.: Pattern recognition methodologies for pollen grain image classification: a survey. Mach. Vision Appl. **33**(1), 18 (2022)
4. Jumanov, I.I., Safarov, R.A.: Algorithms for image processing of micro-objects of medical diagnostics systems. In: International Russian Smart Industry Conference (SmartIndustryCon), pp. 867–872. IEEE (2025). https://doi.org/10.1109/SmartIndustryCon65166.2025.10986021
5. Tsiknakis, N., et al.: Pollen grain classification based on ensemble transfer learning on the Cretan Pollen Dataset. Plants **11**(7), 919 (2022)
6. Garga, B., et al.: Pollen grain classification using some convolutional neural network architectures. J. Imaging **10**(7), 158 (2024)
7. Murphy, D.B., Davidson, M.W.: Fundamentals of Light Microscopy and Electronic Imaging. Wiley, New York (2012)
8. Xing, F., et al.: Deep learning in microscopy image analysis: a survey. IEEE Trans. Neural Netw. Learn. Syst. **29**(10), 4550–4568 (2017)
9. Melanthota, S.K., et al.: Deep learning-based image processing in optical microscopy. Biophys. Rev. **14**(2), 463–481 (2022)
10. Jumanov, I.I., Safarov, R.A.: Optimization of micro-object identification based on a pyramidal model with image segmentation. In: International Russian Smart Industry Conference, pp. 337–342. IEEE (2025). https://doi.org/10.1109/SmartIndustryCon65166.2025.10986135
11. Rezaeilouyeh, H., Mollahosseini, A., Mahoor, M.H.: Microscopic medical image classification framework via deep learning and shearlet transform. J. Med. Imaging **3**(4), 044501–044501 (2016)
12. Buades, A., Coll, B., Morel, J.-M.: Non-local means denoising. Image Process. Online **1**, 208–212 (2011)
13. Murali, V., Sudeep, P.V.: Image denoising using DnCNN: an exploration study. In: Jayakumari, J., Karagiannidis, G.K., Ma, M., Hossain, S.A. (eds.) Advances in Communication Systems and Networks. LNEE, vol. 656, pp. 847–859. Springer, Singapore (2020). https://doi.org/10.1007/978-981-15-3992-3_72
14. Szeliski, R.: Computer Vision: Algorithms and Applications. Springer, Cham (2022). https://doi.org/10.1007/978-3-030-34372-9
15. Jain, A.K., Duin, R.P.W., Mao, J.: Statistical pattern recognition: a review. IEEE Trans. Pattern Anal. Mach. Intell. **22**(1), 4–37 (2000)
16. Shen, D., Wu, G., Suk, H.-I.: Deep learning in medical image analysis. Annu. Rev. Biomed. Eng. **19**, 221–248 (2017)
17. Wang, X.: Deep learning in object recognition, detection, and segmentation. Found. Trends Sig. Process. **8**(4), 217–382 (2016)
18. Warshaneyan, S.S., et al.: Automated Pollen Recognition in Optical and Holographic Microscopy Images: 3rd Cognitive Models and Artificial Intelligence Conference (AICCONF), pp. 1–8. IEEE (2025)

19. Shi, X., et al.: Pollen-YOLO: a deep learning framework for automated pollen identification and its application to palaeoecological reconstruction on the Tibetan plateau. Quaternary **9**(1), 1–6 (2026)
20. Kubera, E., et al.: Detection and recognition of pollen grains in multilabel microscopic images. Sensors **22**(7), 2690 (2022)
21. Bengio, Y., Goodfellow, I., Courville, A.: Deep Learning, vol. 1. MIT Press, Cambridge, MA, USA (2017)
22. Krizhevsky, A., Sutskever, I., Hinton, G.E.: ImageNet classification with deep convolutional neural networks. Commun. ACM **60**(6), 84–90 (2017)
23. Liu, X., et al.: Advances in deep learning-based medical image analysis. Health Data Sci. **2021**, 8786793 (2021)
24. Mamalakis, M., et al.: Artificial Intelligence framework with traditional computer vision and deep learning approaches for optimal automatic segmentation of left ventricle with scar. Artif. Intell. Med. **143**, 102610 (2023)
25. Zangana, H.M., Mustafa, F.M.: From classical to deep learning: a systematic review of image denoising techniques. Jurnal Ilmiah Comput. Sci. **3**(1), 50–65 (2024)
26. Wang, J., et al.: A review of deep learning on medical image analysis. Mob. Netw. Appl. **26**(1), 351–380 (2021)
27. El Helou, M., Süsstrunk, S.: Blind universal Bayesian image denoising with Gaussian noise level learning. IEEE Trans. Image Process. **29**, pp. 4885–4897 (2020)
28. Wang, J., Wang, S., Zhang, Y.: Deep learning on medical image analysis. CAAI Trans. Intell. Technol. **10**(1), 1–35 (2025)
29. Liu, W., Lin, W.: Additive white Gaussian noise level estimation in SVD domain for images. IEEE Trans. Image Process. **22**(3), 872–883 (2012)
30. Tian, C., et al.: Multi-stage image denoising with the wavelet transform. Pattern Recogn. **134**, 109050 (2023)
31. Kovtunenko, V.A., Kunisch, K.: High precision identification of an object: optimality-conditions-based concept of imaging. SIAM J. Control Optim. **52**(1), 773–796 (2014)
32. Liu, P., et al.: Multi-level wavelet-CNN for image restoration. In: Proceedings of the IEEE Conference on Computer Vision and Pattern Recognition Workshops, pp. 773–782 (2018)
33. Jumanov, I.I., Safarov, R.A., Djumanov, O.I.: Optimization of micro-object identification with factorization and correction mechanisms for distorted image points. In: International Russian Smart Industry Conference (SmartIndustryCon), pp. 343–348. IEEE (2025). https://doi.org/10.1109/SmartIndustryCon65166.2025.10986016
34. Wendt, A., Heipke, C.: Simultaneous orientation of brightness, range and intensity images. ISPRS Arch. **36**(5) (2006)
35. Rekeczky, C.: CNN architectures for constrained diffusion based locally adaptive image processing. Int. J. Circuit Theory Appl. **30**(2–3), 313–348 (2002)
36. Peng, L., et al.: Defective pixel corrector for line scan and area scan image sensors. IEEE Trans. Circuits Syst. I: Regular Papers **72**(7), 3325–3337 (2025)
37. Roy, S., Panda, S., Jangid, M.: Modified Reinhard algorithm for color normalization of colorectal cancer histopathology images. In: 29th European Signal Processing Conference (EUSIPCO). IEEE (2021)
38. Shao, L., et al.: Performance evaluation of deep feature learning for RGB-D image/video classification. Inf. Sci. **385**, 266–283 (2017)
39. Coppi, R., Gil, M.A., Kiers, H.A.L.: The fuzzy approach to statistical analysis. Comput. Stat. Data Anal. **51**(1), 1–14 (2006)